A&A 530, A24 (2011)
DOI: 10.1051/0004-6361/201016298

Astronomy & Astrophysics

Fractional polarization as a probe of magnetic fields in the intra-cluster medium

A. Bonafede[1,2,3], F. Govoni[4], L. Feretti[3], M. Murgia[4], G. Giovannini[2,3], and M. Brüggen[1]

[1] Jacobs University Bremen, Campus Ring 1, 28759 Bremen, Germany
e-mail: a.bonafede@jacobs-university.de
[2] Dip. di Astronomia, Univ. Bologna, via Ranzani 1, 40120 Bologna, Italy
[3] INAF- Istituto di Radioastronomia, via Gobetti 101, 40129, Italy
[4] INAF- Osservatorio Astronomico di Cagliari, Loc. Poggio dei Pini, Strada 54, 09012, Capoterra Ca, Italy

Received 10 December 2010 / Accepted 28 February 2011

ABSTRACT

Context. It is now established that magnetic fields are present in the intra-cluster medium (ICM) of galaxy clusters, as revealed by observations of radio halos and radio relics and from the study of the Faraday rotation measures of sources located either behind or within clusters. Deep radio polarization observations of clusters have been performed in the last years, and the properties of the ICM magnetic field have been constrained in a small number of well-studied objects.
Aims. The aim of this work is to investigate the average properties of the ICM magnetic fields, and to search for possible correlations with the ICM thermal properties and cluster radio emission.
Methods. We have selected a sample of 39 massive galaxy clusters from the HIghest X-ray FLUx Galaxy Cluster Sample, and used Northern VLA Sky Survey data to analyze the fractional polarization of radio sources out to 10 core radii from the cluster centers. We have investigated how different magnetic field strengths affect the observed polarized emission of sources lying at different projected distances from the cluster center. In addition, statistical tests are performed to investigate the fractional polarization trends in clusters with different thermal and non-thermal properties.
Results. We find a trend of the fractional polarization with the cluster impact parameter, with fractional polarization increasing at the cluster periphery and decreasing toward the cluster center. Such trend can be reproduced by a magnetic field model with central value of few μG. The logrank statistical test indicates that there are no differences in the depolarization trend observed in cluster with and without radio halo, while the same test indicates significant differences when the depolarization trend of sources in clusters with and without cool core are compared. The comparison between clusters with high and low temperatures does not yields significant differences. Although the role of the gas density should be better accounted for, these results give important indications for models that require a role of the ICM magnetic field to explain the presence of cool core and radio halos in galaxy clusters.

Key words. magnetic fields – radiation mechanisms: non-thermal – polarization – galaxies: clusters: intracluster medium – methods: observational – galaxies: clusters: general

1. Introduction

Increasing attention has been devoted in the last decade to the presence, strength and structure of magnetic fields in galaxy clusters (Ferrari et al. 2008; Carilli & Taylor 2002; Govoni & Feretti 2004; Clarke 2004). In order to understand the physical conditions of the intra cluster medium (ICM) it is important to understand the properties of cluster magnetic fields and their interplay with the other constituents of the ICM. Our current knowledge on cluster magnetic fields comes mainly from radio observations. In some galaxy clusters magnetic fields are revealed by synchrotron emission not obviously associated with any particular galaxy: the so-called radio halos (e.g. Giovannini et al. 2009). Radio halos are wide synchrotron radio sources, characterized by steep spectra[1] ($\alpha > 1$) and low surface brightness ($\sim$1 μJy/arcsec^2 at 1.4 GHz). They are located at the center of galaxy clusters, and are usually found to be unpolarized, the only two exceptions being the cluster Abell 2255 (Govoni et al. 2005; see also Pizzo et al. 2010) and MACS J0717+3745 (Bonafede et al. 2009a). Synchrotron diffuse emission is also observed at the periphery of some galaxy cluster (the so called radio relics, see e.g. Bonafede et al. 2009b; van Weeren et al. 2010) About 30 radio halos are known so far, and all of them are found in clusters with clear signature of on-going or recent merger activity (e.g. Buote 2001; Govoni et al. 2001; Cassano et al. 2010). Shocks and turbulence associated with merger events are expected to inject a considerable amount of energy in the ICM, that could compress and amplify the magnetic field and accelerate relativistic particles, giving thus rise to the observed radio emission. We refer to Ferrari et al. (2008) and Dolag et al. (2008) for recent reviews of the subject.

Estimates of the magnetic field strength have been obtained in clusters where radio halos are observed, under the minimum energy hypothesis (which is very close to equipartition conditions) or by studying the inverse Compton (IC) hard X-ray emission (e.g. Fusco-Femiano 2004; Wik et al. 2009; Ajello et al. 2009; Murgia et al. 2010a). Both of these methods require however several assumptions on the emitting particle distribution and energetic spectrum. In particular the assumptions required by the equipartition approach, in the context of radio halos, strongly affect the resulting estimates. Magnetic field values derived from equipartition and IC indicate that magnetic of $\sim\mu$G level are spread over the cluster volume. Recently, a more sophisticated approach has been applied by Vacca et al. (2010). The authors

[1] $S(\nu) \propto \nu^{-\alpha}$, with α = the spectral index.

investigated the magnetic field power spectrum in the cluster A665 by analyzing the radio halo brightness fluctuations in conjunction with the fractional polarization trend of radio sources at different impact parameters.

Another possibility to investigate the ICM magnetic field properties comes from the study of the Faraday rotation of sources located both behind and within galaxy clusters. Synchrotron radiation from radio galaxies which crosses a magneto-ionic medium is subject to Faraday rotation. The direction of the polarization plane, $\Psi_{\rm int}$, is rotated by a quantity that in the case of a purely external Faraday screen is proportional to the square of the wavelength:

$$\Psi_{\rm obs}(\lambda) = \Psi_{\rm int} + {\rm RM}\lambda^2 \quad (1)$$

$${\rm RM} \propto \int_0^L B_{//} n_{\rm g} {\rm d}l, \quad (2)$$

here $B_{//}$ is the magnetic field component along the line of sight, $n_{\rm g}$ is the ICM gas density and L is the distance along the line of sight. With the help of X-ray observations, providing information about the thermal gas distribution, RM studies give an additional set of information about the magnetic field in the ICM. Recent works have investigated several aspects of the magnetic field morphology, such as its power spectrum (Murgia et al. 2004; Govoni et al. 2006; Bonafede et al. 2010; Vogt & Enßlin 2005; Laing et al. 2008) and its central strength and radial decline (Bonafede et al. 2010). These studies, however, require deep and multi-frequency observations of several sources located at different projected distances from the cluster center, and have thus been performed so far on a small number of clusters. Because of the sensitivity limits of radio telescopes, studies of a large number of galaxy clusters with many RM probes per cluster are still unfeasible with the current instruments. Hence in order to obtain general information on magnetic fields in galaxy clusters without focusing on single objects, another strategy is required.

When synchrotron emission arising from a cluster or background source crosses the ICM, regions with similar $\Psi_{\rm int}$, going through different paths, will be subject to differential Faraday rotation. If the magnetic field in the foreground screen is tangled on scales much smaller than the observing beam, radiation with similar Ψ but opposite orientation will averaged out, and the observed degree of polarization will be reduced (beam depolarization). In the central region of a cluster, the magnetic field is expected to be higher, according to both theoretical studies (see Dolag et al. 2008, for a review) and Faraday RM observation (Clarke 2004; Govoni et al. 2006; Guidetti et al. 2008; Bonafede et al. 2010). Higher value of B and $n_{\rm g}$ result in higher RM, according to Eq. (2). The higher the Faraday RM is, the stronger the beam-depolarization. It is then expected that sources located in projection close to the cluster center will show a lower fractional polarization compared to more distant ones.

Murgia et al. (2004) used the FARADAY code to simulate this effect, proving that a large sample of radio sources could give additional statistical constraints on the intra-cluster magnetic field properties. The advantage of this approach is that there is no need for multi-frequency observations. This effect can be investigated with radio surveys at a single frequency, performed in full polarization mode. Such studies do not provide detailed information on magnetic fields in specific clusters, but allow us to understand the average properties of magnetic fields in the ICM.

In this paper, we present a statistical study of magnetic fields in galaxy clusters. Starting from a sample of clusters selected from the HIghest X-ray FLUx Galaxy Cluster Sample (HIFLUGCS, Reiprich & Böhringer 2002), we use the NRAO Northern VLA Sky Survey (NVSS, Condon et al. 1998) to study the polarization properties of sources located at different impact parameters with respect to the cluster center.

The paper is organized as follows: in Sect. 2 we present the cluster sample, in Sect. 3 radio data are analyzed; The polarization properties of the radio sources are studied in Sect. 4, and used to derive the average magnetic field properties (Sect. 5) with the help of numerical simulations. In Sects. 6–8 the difference in magnetic fields in clusters with and without radio halos and with high and low temperature are investigated. Finally, conclusions are presented in Sect. 9. In this work we assume a ΛCDM cosmological model, characterized by $\Omega_\Lambda = 0.7$, $\Omega_{\rm m} = 0.3$ and $H_0 = 70\ {\rm km\,s^{-1}\,Mpc^{-1}}$.

2. Selection of the clusters

From the HIghest X-ray FLUx Galaxy Cluster Sample (HIFLUGCS) by Reiprich & Böhringer (2002), we selected all objects with $L_{\rm X}[0.1{-}2.4\ {\rm keV}] \geq 1.5 \times 10^{44}$ erg/s. The limit in X-ray luminosity is aimed at selecting massive galaxy clusters, and at the same time having enough clusters to build up a statistical sample. In massive galaxy clusters the magnetic field is expected to be higher, so that the depolarization effect should be more prominent. There are 39 clusters in the HIFLUGCS sample that satisfy this criterion. Using the $L_{\rm X} - M_{200}$ relation obtained by Rykoff et al. (2008) this limit corresponds to $M_{200} \geq 3 \times 10^{14}\ M_\odot/h_{70}$. The HIFLUGCS sample is a X-ray selected and X-ray flux-limited galaxy cluster sample from the ROSAT All-Sky-Survey catalogue. The large FOV of the ROSAT PSPC covers most of the clusters out to r_{500}, which is the radius at which the mean density of the cluster is 500 times that of a critical density. The selection criterion that we used, based on the cluster X-ray luminosity only, guarantees that clusters in different dynamical states are included in our sample.

The HIFLUGCS sample has been used to perform several studies regarding the scaling relations of galaxy clusters (e.g. Chen et al. 2007). Their surface brightness profiles have been derived from pointed ROSAT PSPC (32 clusters) and RASS (7 clusters) observations (Reiprich & Böhringer 2002) by using the standard β-model (Cavaliere & Fusco-Femiano 1976). From X-ray observations the cluster mean temperature T and the gas density distribution have been derived. The gas density distribution is described by the following equation:

$$n_{\rm g}(r) = n_0 \left(1 + \frac{r^2}{r_{\rm c}^2}\right)^{-\frac{3}{2}\beta}, \quad (3)$$

here r is the distance from the cluster center and $r_{\rm c}$ is the cluster core radius.

The basic properties of the clusters in the sample, taken from Reiprich & Böhringer (2002) and rescaled to the cosmological model adopted in this work, are given in Tables 1 and 2. In the same Table, we list the dynamical state of the clusters as found in the literature, indicating clusters with merging signature (M), and with mild or strong cool core (CC).

3. Radio data

Radio images of the selected clusters were retrieved from the Northern VLA Sky Survey (Condon et al. 1998). The NVSS was performed at 1.4 GHz, with a 100 MHz bandwidth, and covers the sky north of $\delta = -40$ deg. The survey was performed

Table 1. Cluster sample selected from the HIFLUGCS catalogue.

Cluster name	RA (J2000)	Dec (J2000)	z	Angular to linear conversion scale $''$/kpc
2A0335	$03^m38^m35.3$	$+09^d57^m55^s$	0.0349	0.6950
A0085	$00^m41^m37.8$	$-09^d20^m33^s$	0.0556	1.0800
A0119	$00^m56^m21.4$	$-01^d15^m47^s$	0.0440	0.8660
A0133	$01^m02^m39.0$	$-21^d57^m15^s$	0.0569	1.1030
A0399	$02^m57^m56.4$	$+13^d00^m59^s$	0.0715	1.3630
A0401	$02^m58^m56.9$	$+13^d34^m56^s$	0.0748	1.4240
A0478	$04^m13^m20.7$	$+10^d28^m35^s$	0.0900	1.6790
A0496	$03^m51^m58.6$	$-22^d10^m05^s$	0.0328	0.6550
A0754	$09^m08^m50.1$	$-09^d38^m12^s$	0.0528	1.0290
A1644	$12^m57^m14.8$	$-17^d21^m13^s$	0.0474	0.9300
A1650	$12^m58^m46.2$	$-01^d45^m11^s$	0.0845	1.5870
A1651	$12^m59^m22.9$	$-04^d11^m10^s$	0.0860	1.6120
A1736	$13^m26^m52.1$	$-27^d06^m33^s$	0.0461	0.9050
A1795	$13^m49^m00.5$	$+26^d35^m07^s$	0.0616	1.1880
A2029	$15^m10^m56.0$	$+05^d44^m41^s$	0.0767	1.4530
A2065	$15^m22^m42.6$	$+27^d43^m21^s$	0.0721	1.3730
A2142	$15^m58^m16.1$	$+27^d13^m29^s$	0.0899	1.6770
A2147	$16^m02^m17.2$	$+15^d53^m43^s$	0.0351	0.6980
A2163	$16^m15^m34.1$	$-06^d07^m26^s$	0.2010	3.3130
A2199	$16^m28^m38.5$	$+39^d33^m06^s$	0.0302	0.6050
A2204	$16^m32^m45.7$	$+05^d34^m43^s$	0.1523	2.6480
A2244	$17^m02^m44.0$	$+34^d02^m48^s$	0.0970	1.7950
A2255	$17^m12^m31.0$	$+64^d05^m33^s$	0.0800	1.5100
A2256	$17^m03^m43.5$	$+78^d43^m03^s$	0.0601	1.1610
A2597	$23^m25^m18.0$	$-12^d06^m30^s$	0.0852	1.5980
A3558	$13^m27^m54.8$	$-31^d29^m32^s$	0.0480	0.9410
A3562	$13^m33^m31.8$	$-31^d40^m23^s$	0.0499	0.9760
A3571	$13^m47^m28.9$	$-32^d51^m57^s$	0.0397	0.7860
A4059	$23^m56^m40.7$	$-34^d40^m18^s$	0.0460	0.9040
COMA	$12^m59^m48.7$	$+27^d58^m50^s$	0.0232	0.4680
HYDRA-A	$09^m18^m30.3$	$-12^d15^m40^s$	0.0538	1.0470
MKW3S	$15^m21^m50.0$	$+07^d42^m32^s$	0.0450	0.8850
ZwCl1215	$12^m17^m41.4$	$+03^d39^m32^s$	0.0750	1.4240

Notes. Column 1: cluster name; Cols. 2, 3: cluster center (RA, Dec); Col. 4: redshift; Col. 5: angular scale.

in full polarization mode, so that the total intensity radio flux (Stokes I) and Stokes Q and U images are provided. The images all have a resolution of $\theta = 45''$ at the FWHM and nearly uniform sensitivity. Their noise rms brightness fluctuations are $\sigma_I \sim 0.45$ mJy/beam (Stokes I) and $\sigma_{U,Q} \sim 0.30$ mJy/beam in Stokes Q and U. Radio images for each cluster are centered on the cluster X-ray peak and have sizes of $20\ r_c \times 20\ r_c$.

The clusters S1101, A3391, A3667, A3266, A3158 and A3112 lying at $\delta < 40$ deg are not in the NVSS, so that the radio sample consists finally of 33 clusters. Coma is the nearest cluster of the sample, with $z = 0.0232$, while Abell 2163 is the most distant one, with $z = 0.2010$. Given the resolution of the NVSS this translates into a linear resolution ranging from 21 kpc to 150 kpc. This guarantees that effects due to the beam depolarization should be visible at the NVSS resolution, provided that the magnetic field is tangled on scales smaller than these. Except of Abell 2163 and Abell 2204, the clusters lie all at $z < 0.1$, their mean redshift is 0.066 with a rms dispersion of 0.032.

From Stokes U and Q images the polarization intensity and polarization angle images were produced:

$$P = \sqrt{U^2 + Q^2}$$
$$\Psi = \frac{1}{2}\arctan\frac{U}{Q}, \quad (4)$$

where P was corrected for the positive bias.

Although the NVSS radio images have a nearly uniform sensitivity, local regions of poorer sensitivity may be present for instance because of dynamic range limitations. In order to avoid including in our source sample peaks of the noise fluctuations, only sources brighter than $5\sigma_I$ in total intensity images were considered. We blanked the total intensity images at $5\sigma_I$, and used these blanked images as a mask to blank the polarization intensity images. We considered only sources that are wider than one beam area. This prevents us from including only the brightest part of low brightness sources, which could bias the sample toward higher F_P values. We then computed the mean polarized intensity flux and the mean total intensity flux for each source, and derived the fractional polarization as $F_P = P/I$.

3.1. Source detection and upper limits

Not all of the sources detected in total intensity are also detected in polarization. In order to fix the flux-threshold in polarization to distinguish between detection and upper-limit, we proceeded as follows: in the NVSS images we have randomly chosen regions where no sources were detected in total intensity. These empty regions have been selected to have an area ≥than one beam, to mimic the same conditions of the detected sources. We have then computed the mean polarized intensity flux, and compared the distribution of "real-sources" and "noise-sources" (see Fig. 1). The threshold was fixed at the value of P where the number of "noise-sources" is less than 10% than the

Table 2. Cluster sample: thermal properties.

Cluster name	L_x [0.1–2.4 keV] 10^{44} erg/s	r_c kpc	n_0 10^{-2} cm^{-3}	β	T keV	Radio	State
2A0335	2.53	24^{+0}_{-0}	$5.29^{+0.06}_{-0.06}$	$0.575^{0.004}_{0.003}$	$3.01^{+0.07}_{-0.07}$		CC[a]
A0085	5.28	60^{+2}_{-2}	$2.43^{+0.09}_{-0.09}$	$0.532^{0.004}_{0.004}$	$6.10^{+0.20}_{-0.20}$		CC[a]
A0119	1.79	365^{+19}_{-18}	$0.14^{+0.01}_{-0.01}$	$0.675^{0.026}_{0.023}$	$5.80^{+0.60}_{-0.60}$		M[b]
A0133	1.59	33^{+0}_{-0}	$2.65^{+0.08}_{-0.08}$	$0.530^{0.004}_{0.004}$	$3.80^{+2.00}_{-0.90}$		CC[a]
A0399	3.87	332^{+96}_{-73}	$0.21^{+0.04}_{-0.03}$	$0.713^{0.0137}_{0.095}$	$7.40^{+0.70}_{-0.70}$	H[h1]	M [p]
A0401	6.90	182^{+8}_{-7}	$0.56^{+0.05}_{-0.04}$	$0.613^{0.010}_{0.010}$	$8.30^{+0.50}_{-0.50}$	H[h2]	M [P]
A0478	9.86	73^{+1}_{-1}	$3.26^{+0.14}_{-0.13}$	$0.613^{0.004}_{0.004}$	$7.10^{+0.40}_{-0.40}$		CC[a]
A0496	2.03	21^{+0}_{-0}	$3.94^{+0.28}_{-0.25}$	$0.484^{0.003}_{0.003}$	$4.13^{+0.08}_{-0.08}$		CC[a]
A0754	2.15	175^{+12}_{-11}	$0.42^{+0.02}_{-0.02}$	$0.698^{0.027}_{0.024}$	$9.00^{+0.05}_{-0.05}$	H[h3]	M[o]
A1644	2.07	218^{+93}_{-67}	$0.27^{+0.08}_{-0.06}$	$0.579^{0.111}_{0.074}$	$4.70^{+0.90}_{-0.70}$		M[c]
A1650	4.05	209^{+77}_{-52}	$0.40^{+0.08}_{-0.06}$	$0.704^{0.131}_{0.081}$	$5.60^{+0.60}_{-0.60}$		D [q]
A1651	4.44	134^{+6}_{-6}	$1.01^{+0.06}_{-0.06}$	$0.643^{0.014}_{0.013}$	$6.30^{+0.50}_{-0.50}$		CC[a]
A1736	1.72	273^{+129}_{-94}	$0.12^{+0.04}_{-0.02}$	$0.542^{0.147}_{0.092}$	$3.50^{+0.40}_{-0.40}$		M[d]
A1795	5.49	57^{+0}_{-0}	$2.71^{+0.05}_{-0.05}$	$0.596^{0.003}_{0.002}$	$6.00^{+0.30}_{-0.30}$		CC[a]
A2029	9.53	61^{+1}_{-1}	$3.62^{+0.14}_{-0.14}$	$0.582^{0.004}_{0.004}$	$8.70^{+0.30}_{-0.30}$		CC[a]
A2065	3.05	509^{+266}_{-137}	$0.19^{+0.07}_{-0.04}$	$1.162^{0.737}_{0.282}$	$5.40^{+0.30}_{-0.30}$		M[e]
A2142	11.89	114^{+3}_{-3}	$1.48^{+0.06}_{-0.06}$	$0.591^{0.006}_{0.006}$	$8.80^{+0.60}_{-0.60}$		CC[a]
A2147	1.54	172^{+74}_{-46}	$0.16^{+0.04}_{-0.03}$	$0.444^{0.071}_{0.046}$	$4.91^{+0.28}_{-0.28}$		M[f]
A2163	20.87	405^{+23}_{-22}	$0.44^{+0.02}_{-0.02}$	$0.796^{0.030}_{0.028}$	$13.29^{+0.64}_{-0.64}$	H[h5]	M[h5]
A2199	2.19	100^{+7}_{-6}	$0.81^{+0.03}_{-0.03}$	$0.655^{0.019}_{0.021}$	$4.10^{+0.08}_{-0.08}$		CC[a]
A2204	15.84	51^{+2}_{-1}	$4.40^{+0.10}_{-0.10}$	$0.597^{0.008}_{0.007}$	$7.21^{+0.25}_{-0.25}$		CC[a]
A2244	4.75	93^{+7}_{-7}	$1.09^{+0.05}_{-0.05}$	$0.607^{0.016}_{0.015}$	$7.10^{+5.00}_{-2.20}$		CC[a]
A2255	3.04	440^{+26}_{-23}	$0.17^{+0.02}_{-0.02}$	$0.797^{0.033}_{0.030}$	$6.87^{+0.20}_{-0.20}$	H[h4]	M[i]
A2256	5.05	432^{+28}_{-26}	$0.25^{+0.01}_{-0.01}$	$0.914^{0.054}_{0.047}$	$7.50^{+0.40}_{-0.40}$	H[h6]	M[l]
A2597	3.82	42^{+1}_{-1}	$3.34^{+0.07}_{-0.06}$	$0.633^{0.008}_{0.008}$	$3.60^{+0.20}_{-0.20}$		CC[a]
A3558	3.54	163^{+3}_{-3}	$0.44^{+0.01}_{-0.01}$	$0.580^{0.006}_{0.005}$	$5.50^{+0.30}_{-0.30}$		M[g]
A3562	1.67	71^{+3}_{-3}	$0.55^{+0.02}_{-0.02}$	$0.472^{0.006}_{0.006}$	$5.16^{+0.16}_{-0.16}$	H[h7]	M[m]
A3571	4.32	131^{+4}_{-4}	$1.05^{+0.09}_{-0.08}$	$0.613^{0.010}_{0.010}$	$6.90^{+0.30}_{-0.30}$		CC[a]
A4059	1.54	65^{+3}_{-3}	$1.13^{+0.08}_{-0.08}$	$0.582^{0.001}_{0.001}$	$4.10^{+0.30}_{-0.30}$		CC[a]
COMA	4.13	247^{+15}_{-14}	$0.29^{+0.06}_{-0.06}$	$0.654^{0.019}_{0.021}$	$8.38^{+0.34}_{-0.34}$	H[h8]	M[n]
HYDRA-A	3.19	36^{+0}_{-0}	$3.40^{+0.35}_{-0.32}$	$0.573^{0.003}_{0.003}$	$3.80^{+0.20}_{-0.20}$		CC[a]
MKW3S	1.53	48^{+1}_{-1}	$1.81^{+0.24}_{-0.24}$	$0.581^{0.008}_{0.007}$	$3.50^{+0.20}_{-0.20}$		CC[a]
ZwCl1215	2.88	319^{+20}_{-18}	$0.25^{+0.01}_{-0.01}$	$0.819^{0.038}_{0.034}$	$5.58^{+0.89}_{-0.78}$		M[h]

Notes. Column 1: cluster name; Col. 2: X-ray luminosity in the 0.1–2.4 keV band; Col. 3: cluster core radius; Col. 4: central density; Col. 5: β parameter; Col. 6: cluster mean temperature; Col. 7: radio emission. H = giant radio halo detected; Col. 8: dynamical state. CC = cool-core cluster, M = merging system, D = debated, see explanation below. If not specified, data are from Chen et al. (2006). Quantities have been corrected for the cosmological model assumed in this paper.

References. [a] Chen et al. (2007), [b] Whitaker et al. (2003), [c] Reiprich et al. (2004), [d] Bozkurt et al. (2009), [e] Bourdin & Mazzotta (2008), [f] Krempeć-Krygier et al. (2002) and Dickey (1997), [g] Rossetti et al. (2007), [h] Rines & Diaferio (2006), [i] Miller & Owen (2003), [l] Sun et al. (2002), [m] Finoguenov et al. (2004), [n] Neumann et al. (2003), [o] Markevitch et al. (2003), [p] Bourdin & Mazzotta (2008), [q] no cool core according to Chen et al. (2006), but the cluster is found to be in a relaxed state with a moderate cool core, by the analysis of Takahashi & Yamashita (2003), [h1] Murgia et al. (2010b), [h2] Bacchi et al. (2003), [h4] Harris et al. (1980), [h3] Kassim et al. (2001), [h5] Herbig & Birkinshaw (1994), Feretti et al. (2001), [h6] Bridle & Fomalont (1976), [h7] Venturi et al. (2000), [h8] Hanisch & Erickson (1980).

number of "real-sources". This ensures that we are safely dominated by detections at every P. The threshold corresponds to $P_t = 0.45$ mJy/beam so when $P \leq P_t$ mJy/beam a 1-σ upper-limit for F_P was derived: $F_P \leq \sqrt{\frac{P_t^2}{(I^2-\sigma_I^2)}}$.

The final sample of sources consists of 696 sources, 334 of which are upper limits.

4. Depolarization analysis

The large sample of sources obtained by the NVSS catalogue allows us to investigate how the depolarization changes as a function of the projected distance from the cluster center.

A radial decline of the magnetic field proportional to n^η is expected from magneto-hydrodynamical simulations performed with different codes (Dolag et al. 2005, 1999; Brüggen et al. 2005; Dubois & Teyssier 2008; Collins et al. 2010) as a result of the compression of thermal plasma during the cluster gravitational collapse. In addition, the comparison between thermal and radio profile brightness (Govoni et al. 2001) also suggests that the non-thermal component follows the distribution of the thermal gas. Here we will assume that the magnetic field radial profile is proportional to the gas density profile, according to:

$$B(r) = \langle B_0 \rangle \left(\frac{n}{n_0}\right)^\eta, \quad (5)$$

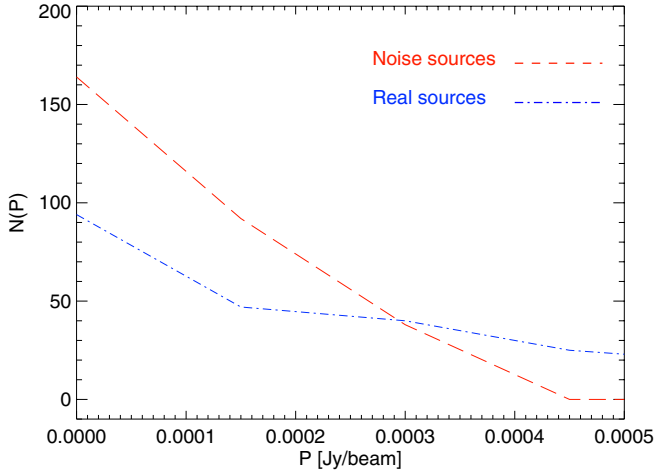

Fig. 1. Number of sources and noise as a function of the observed polarized intensity. Note that the plot is shown only in the range 0–0.0005 Jy/beam, where sources and noise distribution intersect.

where η is a parameter. Given this assumption, the different values of r_c for the clusters in our sample have to be accounted for. The gas density profile (Eq. (3)) is almost constant for $r < r_c$ and decrease faster as $r > r_c$. We have normalized the distance of the sources to the cluster core radius, defining $r_{\rm norm} = r/r_c$. In the upper panel of Fig. 2 the depolarization percentage as a function of $r_{\rm norm}$ is reported for all the sources and the upper limits in our sample.

4.1. Fractional polarization trend

The sample of sources that we have obtained is affected by the presence of non-detections, or censored data. Censored data points are those whose measured properties are not known precisely, but are known to lie above or below some limiting sensitivity. Here a non-detection still gives us the useful information that the P flux (and so the fractional polarization) is below a certain threshold. We have thus a left-censored sample of data. Our aim is to derive the depolarization trend of the sample of sources we have selected, taking care of the information given by censored data.

An extensive field of statistics called "survival analysis" of "lifetime data" exists to address problems of this kind. A very useful statistical estimator in the survival analysis is the Kaplan Meier (KM) estimator, that is described by Feigelson & Nelson (1985). It is a non parametric maximum likelihood type estimator of the distribution function $F(t)$, with t being a generic variable, in our case F_P. It is usually expressed in term of the survival function $S(t)$. Let $x_1 < x_2 < .... < x_r$ denote the distinct, ordered, observed values, the KM estimator is given by[2]:

$$S_{\rm KM}(t) = Prob(T \geq t) = 1 - F(t) \quad (6)$$

$$= \Pi_{i,x_i<t}\left(1 - \frac{d_i}{n_i}\right)^{\delta_i}, \text{ when } t > x_1 \quad (7)$$

$$= 1, \text{ when } t \leq x_1 \quad (8)$$

[2] Here the KM estimator is expressed in the case of right-censored sample. To obtain an estimator of $F(t)$ for left-censored samples we have computed $P(T \leq t) = S_{\rm KM}(M - t)$), with M being the maximum of t_i.

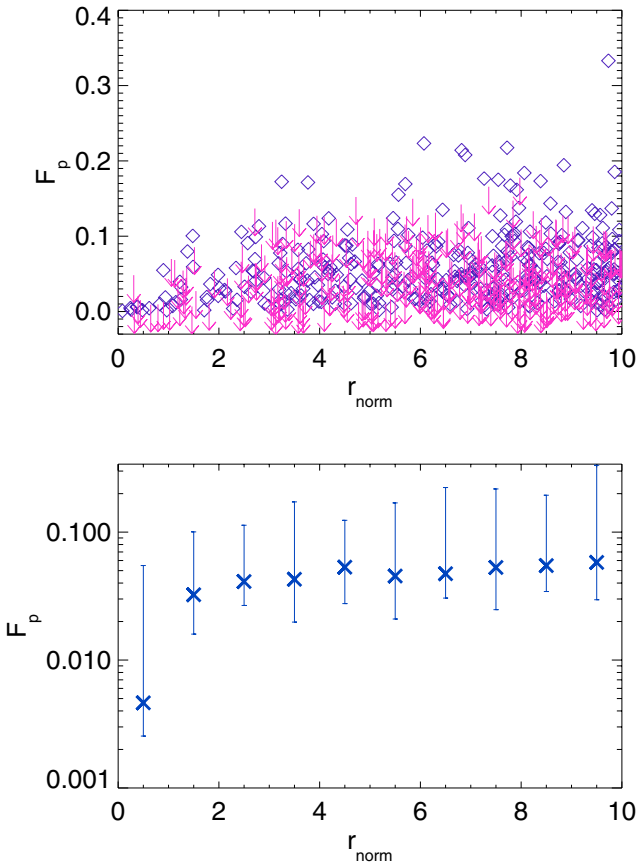

Fig. 2. *Upper panel*: fractional polarization for the sources belonging to the cluster sample as a function of the projected distance from the cluster center normalized by the core radius. The arrows indicate upper limits. *Lower panel*: the median of the KM estimator in every bin is shown, error bars refer to the 16th and 84th percentile of the KM distribution.

with n_i being the number of objects (detected or undetected) $\geq x_i$, d_i are the number of objects at value x_i, and $\delta_i = 1, 0$ if x_i is detected or undetected respectively.

Using the KM estimator, we have derived the distribution function of our data set in each bin. In the lower panel of Fig. 2 the median of the distribution function in each bin is reported. The error bars refer instead to the 16th and 84th percentile of the distribution (those that include 68% of the data in the distribution).

A trend is detected in the F_P going from the cluster center to the cluster outskirts (Fig. 2). The value of F_P in the first bin, i.e. for $r_{\rm norm} < 1$ is 0.0046, and increases gradually in the outer bins. The effect of the cluster on the observed F_P is clear out to ~5 core radii, while in the outer bins, the mean F_P is scattered around a constant value. It reaches values going from 0.047 to 0.058 in the 7th to 10th bin. As the distance from the cluster center increases, RM decreases and the observed F_P is no longer affected by the presence of the ICM.

The value that we find in the outer bin is interpreted as due to depolarization intrinsic to the structure of the radio source as seen by the radio-telescope at this resolution and frequency. We assume that there is no bias in the intrinsic depolarization in all the sources in our sample. The intrinsic fractional polarization is assumed to be the same for sources regardless of their projected

distance from the cluster center, as found e.g. in the Coma cluster (Bonafede et al. 2010).

It follows that internal depolarization should not affect the observed trend of F_p versus $r_{\rm norm}$, but rather act like a constant normalization factor. We further assume that the detected depolarization occurrs in the ICM, meaning neither eventual depolarization internal to the radio-sources nor in their immediate surroundings yield a dominant contribution (see Govoni et al. 2006; Laing et al. 2008; Bonafede et al. 2010; Govoni et al. 2010). The observed trend indicates that magnetic fields are common constituents of galaxy clusters, in agreement with the results by Clarke (2004) and Johnston-Hollitt et al. (2004), who analyzed the Faraday rotation measures of sources located behind and within clusters.

5. Magnetic fields properties

The observed trend of the fractional polarization F_P versus the projected distance from the cluster center can be used to constrain the magnetic field properties. Both the strength and the morphology (i.e. the power spectrum) of the magnetic fields affect the Faraday RM of radio sources, and the consequent beam depolarization that we are investigating here.

We use 3D simulations of random magnetic fields, performed with FARADAY code (Murgia et al. 2004) to simulate the expected trend of F_P for different magnetic field configurations. In this section the magnetic field modeling is briefly presented, and the comparison with the observed sample is performed.

5.1. Magnetic field modeling

The FARADAY code (Murgia et al. 2004) simulates 3D models for the magnetic field in galaxy clusters, and computes the expected RM for radio sources within/behind the cluster.

Numerical simulations start by considering a power-law power spectrum for the vector potential $\boldsymbol{A}$ in the Fourier domain:

$$|A_k|^2 \propto k^{-\zeta} \tag{9}$$

and extract random values of its amplitude A and phase ϕ. The amplitude A is randomly extracted from a Rayleigh distribution (in order to obtain a Gaussian distribution for the real magnetic field components), while ϕ varies randomly from 0 to 2π. Here k is the wave vector in the Fourier domain. The correspondent quantity in the real space is $\Lambda = \frac{2\pi}{k}$. The magnetic field components in the Fourier space are obtained by computing the cross-product:

$$\tilde{B}(k) = \mathrm{i}k \times \tilde{A}(k). \tag{10}$$

Finally, the field components B_i in the real space are derived using a 3D fast Fourier transform inversion. The numerical magnetic field model is then divergence-free, Gaussian random, and isotropic. The power spectrum normalization is set such that the average magnetic field strength follows Eq. (5). This operation is performed in the real space domain, to reduce the computational burden. The same approach has already been used in several works (Murgia et al. 2004; Laing et al. 2008; Guidetti et al. 2008; Bonafede et al. 2010; Vacca et al. 2010).

The adopted power spectrum power law introduces three free parameters: n, $\Lambda_{\rm min}$ and $\Lambda_{\rm max}$. Two more free parameters are introduced once the magnetic field profile (Eq. (5)) is considered: $\langle B_0 \rangle$ and η. Two main degeneracies affect these parameters: the first one concerns the power spectrum, and in particular the values of n and $\Lambda_{\rm max}$, and another degeneracy affects $\langle B_0 \rangle$ and η. Different combinations of n and $\Lambda_{\rm max}$ as well as $\langle B_0 \rangle$ and η lead to similar values of fractional polarization, since it depends mainly on the amount of Faraday rotation measures that originates in the ICM causing the beam depolarization.

Given the number of free parameters, we have fixed the magnetic field radial profile slope (η), and for three different magnetic field power spectra we have investigated the magnetic field strength at the cluster center.

The magnetic field power spectrum is assumed to be Kolmogorov-like. Different independent analyses of RM data (Vogt & Enßlin 2005; Guidetti et al. 2008; Bonafede et al. 2010) indicate that the magnetic field power spectrum observed in galaxy clusters is in good agreement with the power law expected by the Kolmogorov theory, which in our 3D notation corresponds to $n = 11/3$. We note that the theory developed by Kolmogorov is applicable incompressible un-magnetized and uniform fluids, so that its application to the case of the ICM of galaxy clusters is all but obvious. Nonetheless, observational data and cosmological simulations indicate that it is a good description of the pseudo-pressure fluctuations (Schuecker et al. 2004), velocity field (Vazza et al. 2009) and magnetic field (Vogt & Enßlin 2005; Guidetti et al. 2008; Bonafede et al. 2010) in the ICM. Although other spectral slope are not excluded by data, we will adopt here a Kolmogorov like power spectrum. The power spectrum maximum and minimal scale were set to reproduce a magnetic field power spectrum having an auto-correlation length $\Lambda_B \sim 164$ kpc (model 1), $\Lambda_B \sim 25$ kpc (model 2) and $\Lambda_B \sim 8$ kpc (model 3). We then adopted $\Lambda_{\rm min} = 8$ kpc, much smaller than the beam linear size. The values of $\Lambda_{\rm max}$ are then 512 kpc (model 1), 64 kpc (model 2), and 14 kpc (model 3). The value of η is set to 0.5. This choice is motivated by recent works (Guidetti et al. 2008; Bonafede et al. 2010) that found the best agreement between simulations and observations when the magnetic field energy density follows the thermal gas density (i.e. $\eta = 0.5$). We then investigated different values of $\langle B_0 \rangle = 1$, 5, and 10 μG.

5.2. Comparison with observed data

Numerical simulations of the magnetic fields have been performed in a cubical box of 1024^3 pixels, with a pixels-size of 2 kpc. The simulated magnetic field is periodic at the grid boundaries, and the computational grid has been replicated to obtain a simulated field of view of $\sim 20\,\langle r_{\rm c} \rangle \times 20 \langle r_{\rm C} \rangle$, with $\langle r_{\rm C} \rangle$ being the mean value of $r_{\rm c}$ for the clusters in the sample weighted by the number of sources in each cluster ($\sim$270 kpc).

Following Murgia et al. (2004) our aim is to compute, for different magnetic field models, the ratio between the polarization obtained after the rotation of the plane of polarization and the intrinsic polarization at a given frequency. This is the quantity that can be compared with the observed F_P, once the effects introduced by observations are considered.

We simulated different magnetic field models and derived the expected F_P for sources located halfway through the cluster at increasing distance from the cluster center. We proceeded as follows:

– we simulated different magnetic field models, with $\langle B_0 \rangle = 1$, 5 and 10 μG, and $\Lambda_B = 8$, 25, and 164 kpc;

- the intrinsic polarization $P_{\rm int}$ of the sources is assumed to be spatially uniform and ordered ($\Psi_{\rm int}$ constant) and its value is set to reproduce the observed value of F_P at $r_{\rm norm} = 01$;
- according to Eq. (2), we derived the synthetic RM images expected for the different magnetic strengths. The integration path goes from 0 (cluster center) to 10 $\langle r_{\rm c}\rangle$. We used $n_0 = 0.004$ cm^{-3}, $\beta = 0.67$ that are the mean values of our sample weighted by the number of sources that are in each cluster. We produced simulated RM images on a 5400×5400 kpc field of view, with a resolution of ∼2 kpc;
- we then computed the expected polarization plane direction according to Eq. (1) and taking into account the effect due to the NVSS finite bandwidth;
- $P_{\rm int}$ and $\Psi_{\rm obs}$ were then converted into the Stokes parameters $Q(\lambda)$ and $U(\lambda)$ following Eq. (4);
- to the simulated images of $Q(\lambda)$ and $U(\lambda)$ we added a Gaussian noise having rms = 0.3 mJy/beam, as the mean NVSS noise for Q and U images. Q and U images were then convolved with a Gaussian beam having major and minor axis ≈42 kpc. This is the linear size corresponding to 45″ at $z = 0.048$ that is the median redshift of the cluster sample weighted by the number of sources in each cluster;
- finally, the synthetic Q and U images were transformed back to P using Eq. (4);
- the trend of simulated and observed P versus $r_{\rm norm}$ have been compared.

The comparison between the simulated and observed F_P trend obtained by averaging data from the clusters in the sample is performed under the following assumptions:

1. the magnetic field is assumed to be a Gaussian random field. This can be incorrect if the magnetic field is intermittent, and characterized by filaments. However, this is a common assumption in this field, and is mainly motivated by the fact that current data are generally too sparse to determine higher order correlation (see e.g. Laing et al. 2008);
2. the magnetic field phases are assumed to be random, which means that the magnetic field is assumed to have no preferred orientation. Again, this may be not the case when individual clusters are analyzed (e.g. M 84, Laing & Bridle 1987) but we are interested in the magnetic field properties averaged over large volumes of several clusters;
3. the power spectrum fluctuations are assumed to vary with the thermal gas density in the ICM, according to Eq. (5).

Under these assumptions, the model that best reproduces the observed trend of F_P, among those considered here, has $\langle B_0\rangle = 5\mu$G (Fig. 3).

The simulated F_P trends for the different magnetic field models are shown in Fig. 3. We are aware that we are probably averaging the F_P produced by slightly different magnetic field models and configurations, and that more refined and cluster specific models should be considered if precise values are needed. Nonetheless, the best-fit model gives a reasonable order of magnitude estimate for the average magnetic field properties in galaxy clusters.

In our best fit model with a central magnetic field $\langle B_0\rangle = 5\ \mu$G, the mean magnetic field over the central Mpc cube, $B_{\langle 1\ {\rm Mpc}\rangle}$, resulting from our best fit model is ∼2.6 μG. A more detailed analysis has been performed for some of the clusters in our sample: Abell 2255 (Govoni et al. 2006), Hydra-A (Vogt & Enßlin 2005; Laing et al. 2008) and Coma (Bonafede et al. 2010). Given the degeneracy between $\langle B_0\rangle$ and η we compare the mean magnetic field over the central Mpc cube, found by the above mentioned authors with the one obtained here. In A2255 and in the Coma cluster Govoni et al. (2006) and Bonafede et al. (2010) find $B_{\langle 1\ {\rm Mpc}\rangle} \sim 1.2\ \mu$G, and $B_{\langle 1\ {\rm Mpc}\rangle} \sim 2\ \mu$G respectively, while the analysis by Vogt & Enßlin (2005) yields $B_{\langle 1\ {\rm Mpc}\rangle} \sim 1\ \mu$G for Hydra A. They are compatible with the value obtained here.

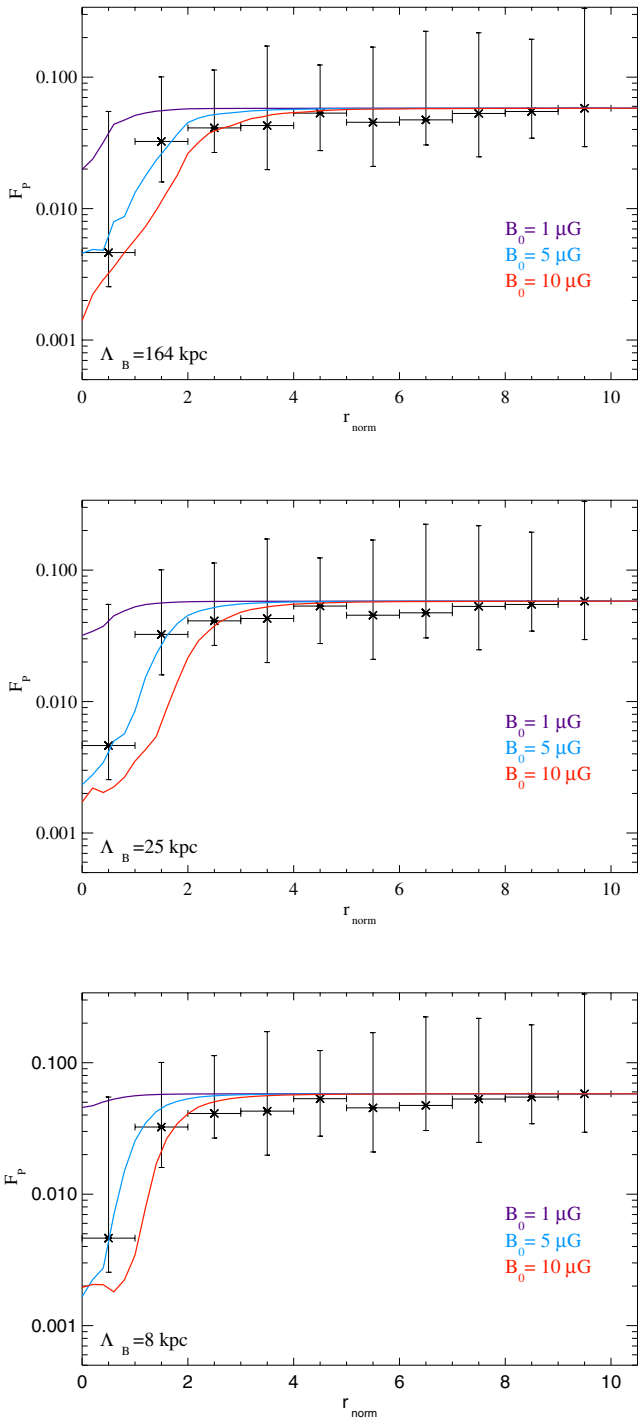

Fig. 3. Simulated (lines) and observed (crosses) depolarization trends for models with different $\Lambda_B = 164$, 25 and 8 kpc (*top, middle* and *bottom panel* respectively). Different colors refer to different magnetic field strengths, as reported in the figures.

6. Dependence of magnetic field properties in clusters with and without radio halo

The sample of clusters that we have selected comprises both virialized and merging systems (see Table 2 and references therein). In a fraction of clusters, with signatures of recent or on-going mergers, a radio halo has been detected (see e.g. Venturi et al. 2008; Giovannini et al. 2009). The origin of these radio sources is still un-known, and two main classes of models have been proposed in the literature:

- *primary or re-acceleration models*: in which electrons are re-accelerated in situ through second-order Fermi mechanism by ICM turbulence developing during cluster mergers (e.g. Brunetti et al. 2001; Petrosian 2001);
- *secondary or hadronic models*: in which electrons originate from hadronic collisions between the long-living relativistic protons in the ICM and thermal ions (e.g. Dennison 1980).

One possibility to explain the presence of radio halos in only a fraction of clusters is to assume different magnetic field strength in the ICM of clusters with and without radio emission. The magnetic field could be amplified during cluster mergers, as indicated by MHD cosmological simulations (see review by Dolag et al. 2008), and then, it could potentially be dissipated once the cluster turns back to the equilibrium state.

6.1. Clusters with and without radio halo

With the aim of investigating a possible difference between the magnetic field properties in clusters with and without radio halos, we have divided our initial sample in two sub-samples, that contain clusters with radio halos (labeled with H in Table 2) and clusters where a giant radio halo (i.e. with size ∼1 Mpc) has not been detected so far. It is worth noting that no upper limits have been put on the radio emission of clusters where a radio halo has not been detected, so that additional care is required to avoid, or at least limit, obvious observational bias.

Most of radio halos have been discovered with follow-up observations of NVSS candidates. Since the NVSS cannot detect large (Mpc) scale emission in clusters at $z < 0.044$, we exclude from our initial sample the clusters with such a redshift. Note that this is a conservative approach, since other single-dish instruments would be clearly able to detect radio emission in these very nearby objects, as in the case of the Coma cluster.

In addition, the radio power of the observed radio halos is usually found to correlate with the cluster X-ray luminosity (e.g. Liang et al. 2000; Feretti et al. 2000). Our sample includes clusters with X-ray luminosities going from 1.5 to 20.8×10^{44} erg/s. Clusters with the lower X-ray luminosity could host halos of lower radio power, that are undetected by present surveys (see e.g. Clarke 2005). It is worth mentioning that recently two radio halos have been found in clusters with low X-ray luminosity, namely 0217+070 (Brown et al. 2011), and A1213 (Giovannini et al. 2009), whose radio power is an order of magnitude or more above the extrapolation of the $L_X - P_R$ correlation at low X-ray luminosities. However, we decided to adopt a conservative approach, and to compare clusters in the same X-ray luminosity range. In Fig. 4, the X-ray luminosity of the clusters in the energy range 0.1–2.4 keV is shown. Clusters are represented with different colors and symbols, depending on the presence of radio halo and on their dynamical state. Objects with $z < 0.044$ have been removed. Clusters with and without radio halo populate the L_X range uniformly. Among the clusters that are known to host a radio halo, the cluster A3562 is the one with the lowest X-ray luminosity: 1.67×10^{44} erg/s. The radio halo was discovered by Venturi et al. (2000) by inspecting NVSS images. We will then consider in the following comparison only clusters with L_X higher than the one of A3562.

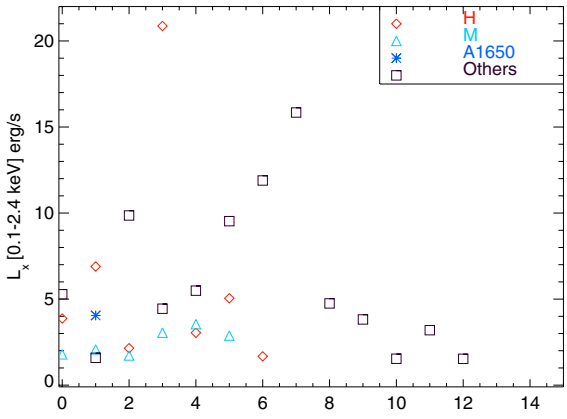

Fig. 4. X-ray luminosity in the 0.1–2.4 keV band for the clusters in the sample here analyzed. Different symbols and colors refer to different sub-samples. Clusters that host a radio halo (red diamonds); clusters where a radio halo has not been detected so far, but with signature of on-going merger according to the literature (cyan triangles), other clusters (squares). The cluster A1650, whose merging state is debated, is signed with a blue asterisk.

Although these two additional criteria should prevent us from obvious observational bias, it is worth mentioning that radio halos with very steep radio spectra and/or low radio brightness could still be present in the cluster labeled as "radio-quiet". Only future instruments, such as LOFAR, will be able to provide a definitive answer. Nonetheless, it is interesting to investigate the properties of the ICM magnetic fields in these two sub-samples, according to our present knowledge about their radio emission. The fractional polarization for the two sub-samples (radio-halo and radio-quiet) is shown in Fig. 5. The halo sample consists of 374 sources (194 of which are upper limits), while the radio-quiet sample consists of 243 sources (112 upper limits).

We want to test the null hypothesis that the two populations, subject to left-censoring, have the same distribution. We performed the logrank statistical test, that is a non-parametric test, widely used in astronomy when censored populations have to be compared.

According to the logrank test, let T_{ij} being the observed value from distribution $i = 1, 2$, with $j = 1...N_i$. Let then $y_1 < y_2 < \ldots < y_r$ with $r \leq N = N_1 + N_2$ denote the uncensored values in the combined samples. Given two independent random samples drawn from populations having distribution functions[3] $F_i(t) = P(T_{ij} \geq t)$ we want to test the null hypotheses $H_0 : F_1(t) = F_2(t)$, for all t. Let $d_{i,j}$ denote the number of objects from sample $i = y_j$, d_j the number of objects from both samples $= y_j$, $n_{i,j}$ the number of objects from sample $i \geq y_j$ and similarly n_j the number of objects from both samples $\geq y_j$. The quantity

$$L_n = \Sigma_{j=1}^{r} \left(d_{1,j} - \frac{d_j n_1}{nj} \right) \quad (11)$$

[3] Here the logrank test is expressed in the case of right-censored sample.

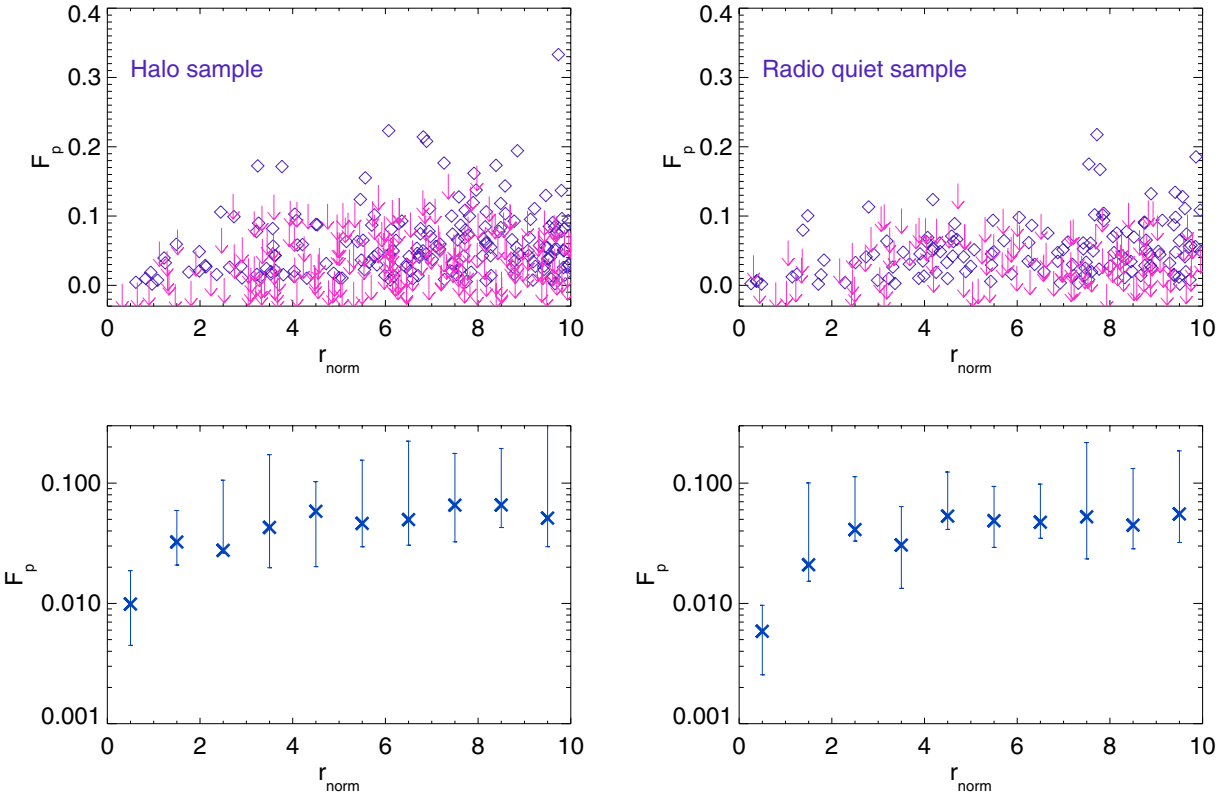

Fig. 5. Fractional polarization versus the projected distance from the cluster center, normalized by the core radius, for sources in clusters that host a radio halo (*left*), and that do not host a radio halo (*right*). Arrows indicate upper limits. *Bottom panel*: crosses refer to the median of the KM estimator is each bin, bars indicate the 14th and 84th percentile. Due to the low number of points in each bin the width of each bin is adaptively set so that at leat 3 detections fall within a bin.

for large N, under H_0, is approximately normally distributed with zero mean and variance σ_n^2. Hence, H_0 is rejected at level α if

$$\left|\frac{L_n}{\sigma_n}\right| \geq z_{\alpha/2} \tag{12}$$

where $z_{\alpha/2}$ is the score such that the area under a standard normal curve over the interval $[-z_{\alpha/2}, z_{\alpha/2}]$ is $1-\alpha$. We refer again to Feigelson & Nelson (1985) for an illustrative explanation of the test with application to astronomical data. Our null hypothesis is that the two populations of F_P in clusters with and without radio halo are different realization of the same sample. The null hypothesis is accepted with high significance: $P = 0.99$. We can conclude that the depolarization trend for sources seen through clusters is the same in these two sub-samples. Since the amount of depolarization depends on the Faraday rotation in the external screen, there are two different possibilities to explain our results:

1. both magnetic field and gas density distributions in cluster with and without radio halos have similar properties; or
2. magnetic field and gas density are both different in clusters with and without radio halo, but conspire to give rise to the same F_P. (i.e. higher magnetic field and lower gas density in one sample and lower magnetic field and higher gas density in the other one).

The mean values of n_0, weighted by the number of sources, for the radio halo and radio quiet samples are 0.003 ± 0.001 cm^{-3} and 0.005 ± 0.010 cm^{-3} respectively. Since they are compatible within errors, we can conclude that there is no evidence for a different magnetic field in clusters with and without radio halos.

6.2. Analysis of the possible contamination by merging effects

Processes related to merger events could change the magnetic field structure in galaxy clusters, increasing the field auto-correlation length and thus also the F_P of the observed sources. Also, if merger events amplify the magnetic field strength, a lower value of F_P is expected. These two effects could conspire to give the same F_P distribution in the radio halo and radio quiet samples even if magnetic field is higher in the radio halo sample, because of the larger auto-correlation length of the magnetic field. In order to prevent this, we have repeated the analysis described in Sect. 6 considering only merging systems in the radio quiet sample. The radio quiet merging sample consists of 203 sources (94 upper limits), and the logrank test yields a probability of 0.70 that the radio halo and radio quiet merging sample are drawn to the same intrinsic population. We can conclude that the depolarization trend is the same in merging clusters, regardless of the presence of a radio halo or not.

6.3. Magnetic field and radio halo origin

The results we have obtained in the previous sections can also be used as a test for the radio halo formation models.

Brunetti et al. (2009) have analyzed the well-known correlations between radio halo power at 1.4 GHz, $P_{1.4}$, and the cluster X-ray luminosity, L_X (e.g. Liang et al. 2000; Giovannini et al. 2009) in a sample of X-ray selected clusters. Among this sample only $\approx\frac{1}{3}$ of clusters host radio halos, while for the other clusters of the sample upper limits on their radio emission have been put (Brunetti et al. 2007). It must be noted that the sample of clusters that they have analyzed is composed of both merging and dynamically relaxed clusters, and that the upper-limits have been computed assuming a value for the radio spectral index. Brunetti et al. (2009) conclude that in the hadronic scenario the energy density of the magnetic field in clusters without a radio halo should be at least 10 times lower than in those that host radio halo emission.

More recently, Keshet & Loeb (2010) have proposed a model within the hadronic scenario, in which cosmic rays diffuse away from their sources (supposed to be supernovae), whereas the magnetic fields are amplified by mergers in clusters with radio halos. The observed bi-modality in the $P_{1.4}$–L_X plane is then attributed to a bi-modality in magnetic field strength for clusters with and without radio halos. Radio halos are associated with clusters having *strong* B, i.e. $B \gg B_{\rm CMB}$ in the radio emitting region, whereas clusters with $B \ll B_{\rm CMB}$ all over their volume would be radio quiet[4].

The result obtained in the previous sections indicates that the bi-modality in the $P_{1.4}$–L_X plane cannot be attributed to a bi-modality in magnetic field properties.

The result we find here is based on a statistical approach, however, previous works have already investigated the magnetic field properties in clusters either with and without radio halo, finding results consistent with those we obtain here. For example, magnetic fields of several μG were inferred in clusters without radio halo by e.g. Clarke et al. (2001), and Murgia et al. (2004), and recently, Govoni et al. (2010) found that clusters seem to follow a common $S_X - RM$ distribution, S_X being the X-ray surface brightness, independently on their radio properties. However, this is the first time that a statistical comparison between magnetic fields in clusters with and without radio emission has been performed and our result is a further indication that hadronic models are difficult to reconcile with present data (Brunetti et al. 2008; and Dallacasa et al. 2009; Donnert et al. 2010; Jeltema & Profumo 2010).

7. Dependence of magnetic field parameters on the presence of a cool core

Galaxy clusters are often divided, according to their X-ray emission, into cool core and non cool core clusters (e.g. Hudson et al. 2010). The former class is characterized by a bright central peak in the cluster X-ray surface brightness, a high central gas density, and a positive gradient of the metal abundance profile. The core is characterized by a radially increasing temperature. Cool core clusters are believed to be systems in dynamical equilibrium, while the energy released by cluster mergers could transform cool core clusters into non cool core systems (see e.g. Motl et al. 2004; Rossetti & Molendi 2010; and references therein). In the core, the cooling time of the gas is much shorter than a Hubble time, but the lack of strong cooling lines revealed by X-ray spectroscopy of *Chandra* and *XMM-Newton*, indicates that the cooling of the gas must be inhibited. Several processes could in principle be responsible for that, such as the presence of heating sources (e.g. Binney & Tabor 1995), or thermal conduction from larger radii, e.g. Narayan & Medvedev 2001). Recently, several authors have investigated the role that magnetic fields could have in this context (e.g. Bogdanović et al. 2009; Ruszkowski & Oh 2010; Parrish et al. 2010).

We will compare here the depolarization trend of sources in clusters with and without cool core. Chen et al. (2007) analyzed the basic properties of the clusters in the HIFLUGCS sample (see Tables 1 and 2 of that paper) and divided the objects in moderate cool core, pronounced cool core and non cool core. Both moderate and pronounced CC are labeled as CC in our Table 2.

We have divided our initial sample into two sub-samples. Since cool core clusters are characterized by the presence of a cD galaxy sitting in the cluster center, while the same is not always true for non cool core cluster clusters, we considered in the non cool core sample only clusters that have a radio galaxy at their center (A1736, A2163, A3558, A3562, COMA, and ZWCL1215). The cool core sample consists of 66 radio sources (30 of them are upper limits), while the non cool core samples comprises 295 sources (165 upper limits). F_P data are shown in Fig. 6. We want to test the null hypothesis that the two populations, subject to left-censoring, have the same distribution. We performed the logrank statistical test, The result of the logrank tests applied to the samples of cool core and non cool core clusters is that the null hypothesis has a small significance ($P = 0.15$). Although the null hypothesis cannot be rejected at 95% confidence level (corresponding to $P = 0.05$), that is the threshold commonly assumed in statistics, the low value of P indicates that the two samples are likely to be realizations of intrinsically different populations. This could be due to a different magnetic field or to the different gas density that characterize the sample (we find a weighted mean of $n_0 = 0.017 \pm 0.013$ for the cool core sample and $n_0 = 0.003 \pm 0.001$ for the non cool core sample), or a combination of the two.

Increasing attention has been devoted in recent years to the role that different magnetic field configurations could have in explaining the observed bi-modality among cool core and non-cool core clusters (see e.g. Parrish et al. 2009; Bogdanović et al. 2009; Parrish et al. 2010; Ruszkowski et al. 2010, and Ruszkowski & Oh 2010). The main idea is that magneto-thermal instabilities could lead to different magnetic field configuration in the ICM depending on the thermal properties of clusters. When $\nabla T \cdot \boldsymbol{g} < 0$, i.e. when the gravity field $\boldsymbol{g}$ is anti-parallel to the temperature gradient in the ICM, heat-driven flux buoyancy instabilities (HBI) are developed. The HBI reorient the magnetic field lines to be perpendicular to the temperature gradient, thus reducing the effective conductivity of the plasma and preventing the cooling catastrophe (Ruszkowski & Oh 2010). Recently, Ruszkowski & Oh (2010) and Parrish et al. (2010) have shown that modest levels of turbulence ($\sim$100 km s^{-1}) can suppress the HBI, resulting in a quasi-stable thermal equilibrium, with isotropically tangled magnetic field lines. However lower levels of turbulence mixing are insufficient to suppress HBI, resulting in a thermal runaway and leading to a cool core cluster. A different magnetic field configuration would then be expected in clusters with and without cool cores, and the combined effects of HBI and turbulence would explain how minor and major mergers could disrupt the cool core.

At the aim of quantify how much of the observed F_P is due to the gas density and magnetic field inside the core, we integrated numerically Eq. (2) from 0 to one core radius and from 1 to 10 core radii, assuming a magnetic field with $\langle B_0 \rangle = 5$ μG, $n_0 = 0.017$ cm^{-3}, $\beta = 0.6$, $r_c = 90$ kpc, that are the weighted means for sources in the cool core sub-sample. The ratio of the

[4] $B_{\rm CMB} = 3.2(1+z)^2 \mu$G is the equivalent magnetic field strength of the cosmic microwave background (CMB).

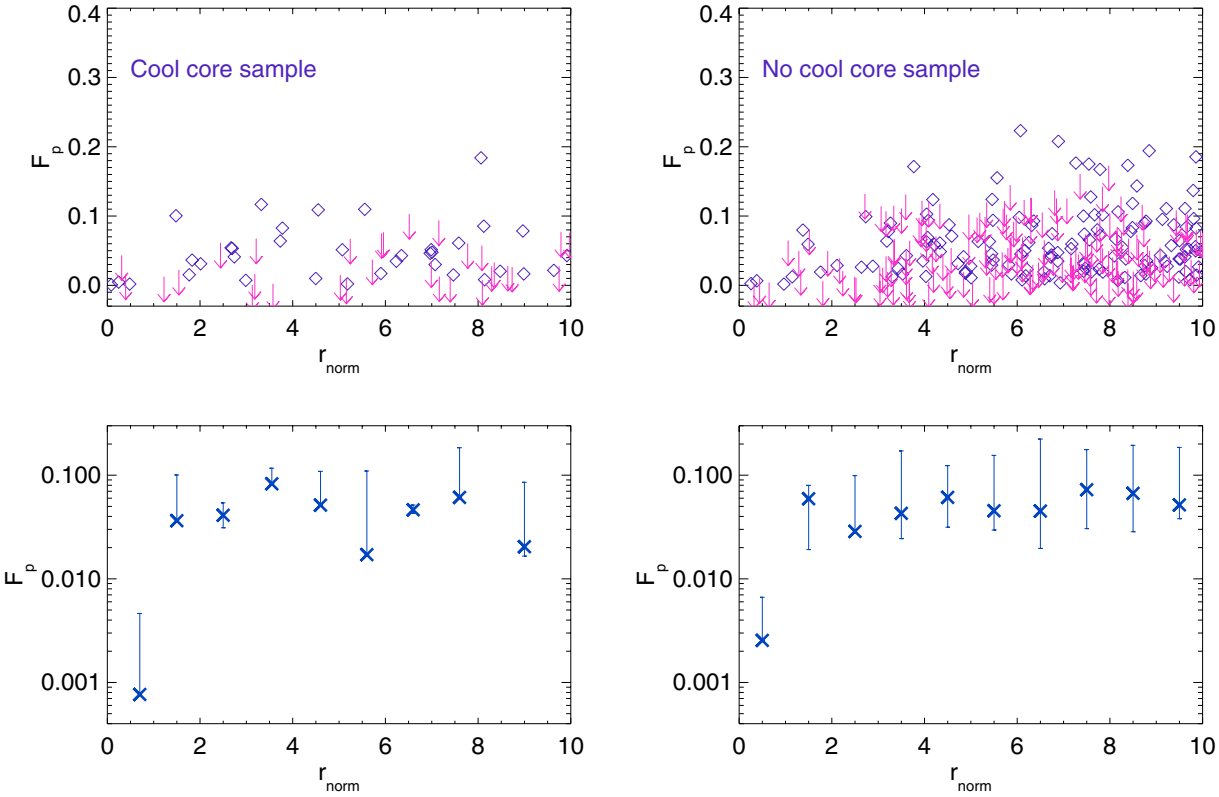

Fig. 6. *Top panel*: fractional polarization versus the projected distance from the cluster center, normalized by the core radius, for sources in cool core clusters (*left*) and non cool core clusters (*right*). Arrows indicate upper limits. *Bottom panel*: crosses refer to the median of the KM estimator is each bin, bars indicate the 14th and 84th percentile. Due to the low number of points in each bin the width of each bin is adaptively set so that at leat 3 detections fall within a bin.

two quantities gives 0.79, indicating that the RM resulting from the core is a consistent fraction of the total amount which is responsible for the observed F_P.

The results we have obtained in this section is not conclusive, but suggest a possible difference in the magnetic field properties of clusters with and without cool cores, thus supporting the scenario proposed by Parrish et al. (2009); Ruszkowski & Oh (2010); Parrish et al. (2010). Unfortunately, these data are not suitable for further investigation (i.e. to disentangle the effects of the gas density and to better investigate if and how the difference in the magnetic field properties of these two samples is due to different magnetic field strengths and structure) but indicate that a more detailed analysis of the magnetic field in these two samples could offer important information about the interplay of magnetic fields, thermal conduction and the bimodality cool core, non cool core clusters. Bogdanović et al. (2011) have shown in fact that Faraday Rotation Measure observations performed with the Extended Very Large Array (EVLA) and with the Square Kilometer Array (SKA) will be able to discern whether the MHD instabilities dominate the dynamics of an ICM, and hence affect the structure of the magnetic field.

8. Magnetic field strength and cluster temperature

Recent works have analyzed a possible connection between the magnetic field strength and the cluster gas density and temperature. These studies are based on cosmological simulations (e.g. Dolag et al. 2005, 1999; Brüggen et al. 2005) or plasma physical considerations (Kunz et al. 2010). SPH simulations predict that the mean magnetic field strength varies with the ICM mean temperature according to $B \propto T^2$. A shallower trend has been found by, Kunz et al. (2010) who found $B \propto T^{3/4}$.

Here we investigate a possible connection between the observed F_P and the cluster temperature. The selection criterion we have used, based on high X-ray luminosity, naturally favors the selection of hot clusters. Nonetheless, clusters in our sample span a good range of temperatures, going from 3 to 13 keV. We have divided our initial sample in two sub-samples having $T > 7$ keV and $T \leq 7$ keV respectively. The cut in temperature is set to have almost the same number of sources in both samples.

The high and low T sub-samples consist of 305 sources (163 upper limits) and 391 sources (171 upper limits), respectively. The trend of F_p versus $r_{\rm norm}$ for these two sub-samples is shown in Fig. 7. The logrank test yields that the null hypotheses should be accepted with $P = 0.64$, thus indicating a common origin for the two population. The mean central gas density n_0 for the two samples is 0.003 ± 0.010 ($T > 7$ keV sample) and 0.004 ± 0.015 ($T \leq 7$ keV sample), meaning that the logrank test on F_P is actually a test on the magnetic field properties, while different values of the gas density should not play an important role.

Recently Govoni et al. (2010) have analyzed the Faraday RM of a sample of sources that belong to hot nearby galaxy clusters, and used these data together with literature ones in order to investigate a possible connection between the magnetic field strength and the cluster mean temperature. Clusters are divided

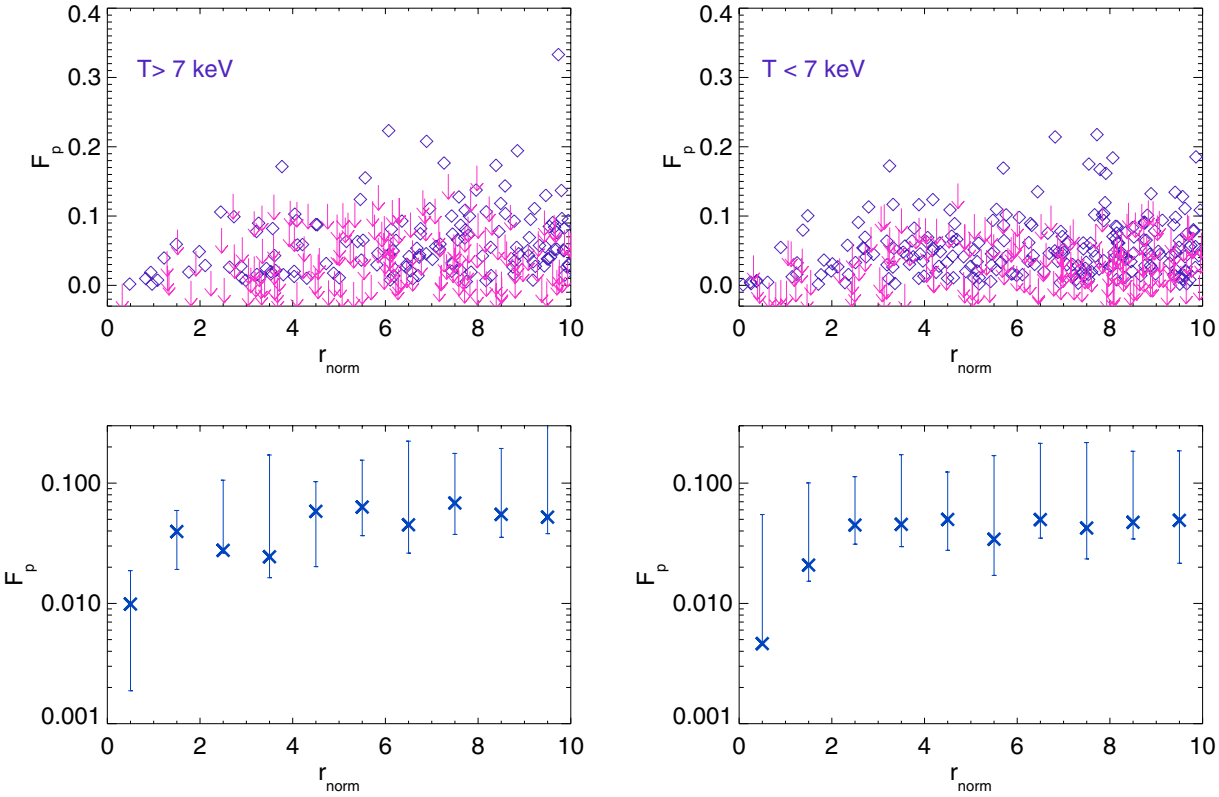

Fig. 7. Fractional polarization versus the projected distance from the cluster center, normalized by the core radius, for sources in clusters with $T \geq 7$ keV (*left*), and clusters with $T \leq 7$ keV (*right*). Arrows indicate upper limits. *Bottom panel*: crosses refer to the median of the KM estimator is each bin, bars indicate the 14th and 84th percentile. Due to the low number of points in each bin the width of each bin is adaptively set so that at leat 3 detections fall within a bin.

into three samples having $T < 4$ keV, $4 \leq T \leq 8$ keV and $T > 8$ keV. The data analyzed do not show evidence for such a correlation, indicating that a possible connection between the magnetic field strength and the gas temperature, if present, is very weak (Govoni et al. 2010). As previously noted, the temperature threshold of 7 keV has been chosen arbitrarily to divide clusters into two sub-samples. In order to compare our results with those of Govoni et al. (2010), we repeated the test comparing clusters with $T \leq 4$ and $T \geq 8$ keV. There are 75 sources (28 upper limits) in clusters with $T \leq 4$ keV and 305 sources (163 upper limits) in clusters with $T \geq 8$ keV. The logrank test indicates that the null hypothesis can be accepted with $P = 0.66$. These data do not indicate a possible difference in the magnetic field properties of clusters depending on their temperature, but due to the small number of sources in the $T \leq 4$ keV sample, a more detailed analysis would be required. We note however that these results are in agreement with those obtained by RM data (Govoni et al. 2010).

9. Conclusions

We performed a statistical analysis of the fractional polarization of radio sources in a sample of X-ray luminous galaxy clusters with the aim of studying the properties of the intra-cluster medium magnetic field. We used data from the NVSS to search for a trend in the fractional polarization with distance from the cluster center, following the approach proposed by Murgia et al. (2004). The sample of clusters we have selected comprises both cool core clusters and merging systems. We have detected a clear trend of the fractional polarization, being smaller for sources close to the cluster center and increasing with increasing distance from the cluster centers. The low fractional polarization in sources closer to the center is interpreted as result of higher beam-depolarization, occurring because of the higher magnetic field and gas density in these regions. We are assuming here that the depolarization occurs in the ICM itself (i.e. that the internal depolarization occuring in the radoiosources and in their immediate surroundings are not dominant, see Govoni et al. 2006; Laing et al. 2008; Bonafede et al. 2010; Govoni et al. 2010;). This result confirms that magnetic fields are ubiquitous in galaxy clusters, as already found by Clarke (2004) and Johnston-Hollitt et al. (2004). Our results can be summarized as follows:

- We used 3D magnetic field simulations performed with the FARADAY code to search for the magnetic field model that best reproduces the trend of the fractional polarization with the distance from the cluster center. We assumed that the magnetic field power spectrum is Kolmogorov-like and that the magnetic field energy density decreases with radius as the gas thermal energy density. Under these assumptions, we found that a magnetic field with a central value of 5 μG gives the best agreement with the observed fractional polarization trend.
- We investigated possible differences between the F_P trend observed in clusters with and without radio halos. The logrank statistical test indicates that the two sample of sources very likely belong to the same intrinsic population ($P = 0.99$). Magnetic fields in galaxy clusters are then likely to share the same properties regardless of the presence of radio

emission from the ICM. This result poses problems for the "hadronic-models" for the origin of radio halos, that requires a difference in magnetic field strengths in clusters with and without radio halos.

– We searched for possible differences in the magnetic field properties in clusters with and without cool core. The logrank test indicates that the F_P distribution observed in clusters with and without cool cores is likely to be different (the null hypothesis of the two samples belonging to the same population has a low significance: $P = 0.15$). This is expected by recently proposed models that explain the cool core and non cool core bimodality in as due to different magnetic field configurations in clusters with and without cool core (Parrish et al. 2009, 2010; Ruszkowski et al. 2010; and Ruszkowski & Oh 2010). The results obtained here must be taken with cautions since the role of the different gas densities in the two samples is not easy to quantify, and could play a crucial role. Deeper radio observations would be required to properly test these models.
– We searched for a possible dependence of magnetic fields from the cluster mean temperature. Clusters were initially divided into two samples having $T \geq 7$ keV and <7 keV. The result of the logrank test yields that the null hypothesis that the two samples are intrinsically drawn from the same population is accepted with $P = 0.64$. In order to compare the F_P analysis with the recent result by Govoni et al. (2010), we repeated the test by dividing the clusters into two samples having $T \geq 8$ keV and $T \leq 4$ keV. The logrank test indicates now that null hypothesis can be accepted with $P = 0.66$. Due to the smaller number of sources in the $T \leq 4$ sample this result would need further investigation, but indicate that clusters with different temperatures share the same magnetic field properties.

Acknowledgements. We thank L. Rudnick for very helpful discussions and precious advices. We also thank V. Vacca, G. Brunetti and U. Keshet for useful discussions, and the referee for his/her useful comments. The Synage++ package was used to perform part of the analysis. This work was supported by the Italian Space Agency (ASI), and by the Italian Ministry for University and research (MIUR). A.B. and M.B. acknowledge support by the DFG Research Unit 1254 "Magnetization of interstellar and intergalactic media: the prospect of low frequency radio observations". This research has made use of the NASA/IPAC Extragalactic Data Base (NED) which is operated by the JPL, California institute of Technology, under contract with the National Aeronautics and Space Administration.

Appendix A: Investigating possible caveats

We will investigate here possible caveats that could affect our analysis of the fractional polarization trend (Sect. 4).

A.1. Cluster sources and background sources

We are analyzing the F_p trend versus the cluster impact parameter, so that in each bin we will have both sources that belong to the cluster and sources that are in its background. The difference in the F_p experienced by a source lying in a plane perpendicular to our line of sight and passing through the cluster center and a source that is in the background of the cluster is a small factor (the dispersion of the RM changes of a factor $\sqrt{2}$), so that we are confident that this should not cause a major effect.

Radio sources that belong to the clusters in our sample could have larger angular sizes with respect to distant background ones. In particular, cluster radio sources sometimes show a "narrow-angle tail" or "wide-angle tail" morphology. Tails are known to be usually less polarized intrinsically, i.e. when observed at high frequencies. In addition, the ICM in the immediate surrounding of cluster radio sources could be locally compressed, so that cluster radio sources could suffer higher depolarization respect to background ones. Given that redshifts are not known for all of the sources in our sample, a possible way to distinguish background and cluster radio sources is to divide them according to their angular size. We have separated the source sample into two samples having size >5 beams and <5 beams, and compared the F_P trends of the two populations. The value of 5 beams was chosen on the basis of the radiosources in the cluster Abell 2255. In this cases in fact the radio sources that are cluster members are known (Miller & Owen 2003), its redshift is representative of the sample, and "narrow-angle tail" and "wide-angle tail" type sources are present in the cluster. The logrank test indicates with high significance ($P = 0.96$) that the two samples have the same properties, so that effects due to local compression of the ICM and source size, as well as projection effects should not play any role. We can then safely consider the sample as a whole, as we did.

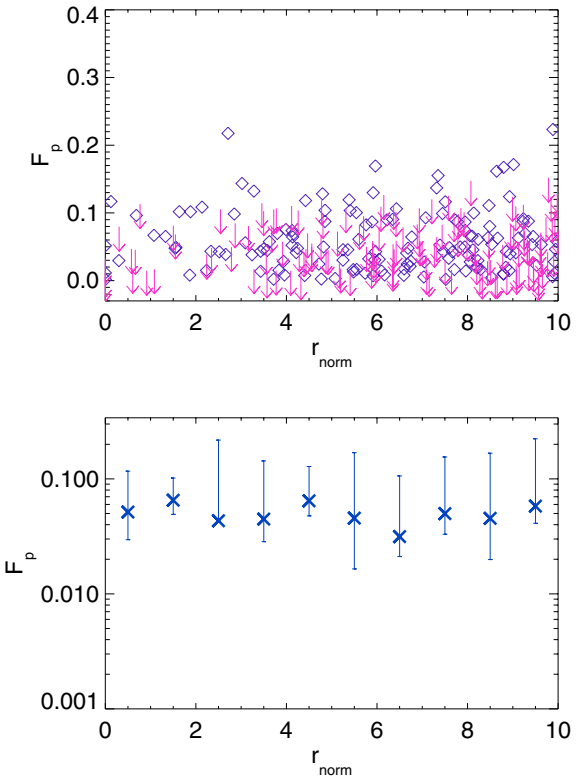

Fig. A.1. Fractional polarization of sources versus projected distance. Sources are centered on a position that is 10 r_c far from the cluster center. Arrows indicate upper limits. *Bottom panel:* crosses refer to the median of the KM estimator is each bin, bars indicate the 14th and 84th percentile. No trend is detected in this case.

A.2. F_P trend and cluster center

Another issue is related to the binning process. The first bin, $r_{\rm norm} < 1$ could show a lower F_p because the number of sources that fall within thin bin is small, and the chance of finding strongly polarized sources in then reduced. To verify this, we repeated the same analysis described in Sect. 4 but centered on different position. The center is now chosen at a distance corresponding to ~10 r_c for each cluster. The F_p distribution is shown in Fig. A.1. No trend is detected now. This

guarantees that the trend detected in Sect. 4 is real and due to the cluster and not to missing statistics.

References

Ajello, M., Rebusco, P., Cappelluti, N., et al. 2009, ApJ, 690, 367
Bacchi, M., Feretti, L., Giovannini, G., & Govoni, F. 2003, A&A, 400, 465
Binney, J., & Tabor, G. 1995, MNRAS, 276, 663
Bogdanović, T., Reynolds, C. S., Balbus, S. A., & Parrish, I. J. 2009, ApJ, 704, 211
Bogdanović, T., Reynolds, C. S., & Massey, R. 2011, ApJ, 731, 7
Bonafede, A., Feretti, L., Giovannini, G., et al. 2009a, A&A, 503, 707
Bonafede, A., Giovannini, G., Feretti, L., Govoni, F., & Murgia, M. 2009b, A&A, 494, 429
Bonafede, A., Feretti, L., Murgia, M., et al. 2010, A&A, 513, A30
Bourdin, H., & Mazzotta, P. 2008, A&A, 479, 307
Bozkurt, M., Hudaverdi, M., & Ercan, E. N. 2009, Publ. Astron. Obs. Belgrade, 86, 347
Bridle, A. H., & Fomalont, E. B. 1976, A&A, 52, 107
Brown, S., Duesterhoeft, J., & Rudnick, L. 2011, ApJ, 727, L25
Brüggen, M., Ruszkowski, M., Simionescu, A., Hoeft, M., & Dalla Vecchia, C. 2005, ApJ, 631, L21
Brunetti, G., Setti, G., Feretti, L., & Giovannini, G. 2001, MNRAS, 320, 365
Brunetti, G., Venturi, T., Dallacasa, D., et al. 2007, ApJ, 670, L5
Brunetti, G., Giacintucci, S., Cassano, R., et al. 2008, Nature, 455, 944
Brunetti, G., Cassano, R., Dolag, K., & Setti, G. 2009, A&A, 507, 661
Buote, D. A. 2001, ApJ, 553, L15
Carilli, C. L., & Taylor, G. B. 2002, ARA&A, 40, 319
Cassano, R., Ettori, S., Giacintucci, S., et al. 2010, ApJ, 721, L82
Cavaliere, A., & Fusco-Femiano, R. 1976, A&A, 49, 137
Chen, Y., Reiprich, T. H., Böhringer, H., Ikebe, Y., & Zhang, Y. 2007, A&A, 466, 805
Clarke, T. E. 2004, J. Kor. Astron. Soc., 37, 337
Clarke, T. E. 2005, in From Clark Lake to the Long Wavelength Array: Bill Erickson's Radio Science, ed. N. Kassim, M. Perez, W. Junor, & P. Henning, ASP Conf. Ser., 345, 227
Clarke, T. E., Kronberg, P. P., & Böhringer, H. 2001, ApJ, 547, L111
Collins, D. C., Xu, H., Norman, M. L., Li, H., & Li, S. 2010, ApJS, 186, 308
Condon, J. J., Cotton, W. D., Greisen, E. W., et al. 1998, AJ, 115, 1693
Dallacasa, D., Brunetti, G., Giacintucci, S., et al. 2009, ApJ, 699, 1288
Dennison, B. 1980, ApJ, 239, L93
Dickey, J. M. 1997, AJ, 113, 1939
Dolag, K., Bartelmann, M., & Lesch, H. 1999, A&A, 348, 351
Dolag, K., Grasso, D., Springel, V., & Trachev, I. 2005, in X-Ray and Radio Connections, ed. L. O. Sjouwerman, & K. K. Dyer
Dolag, K., Bykov, A. M., & Diaferio, A. 2008, Space Sci. Rev., 134, 311
Donnert, J., Dolag, K., Brunetti, G., Cassano, R., & Bonafede, A. 2010, MNRAS, 401, 47
Dubois, Y., & Teyssier, R. 2008, A&A, 482, L13
Feigelson, E. D., & Nelson, P. I. 1985, ApJ, 293, 192
Feretti, L., Brunetti, G., Giovannini, G., Govoni, F., & Setti, G. 2000, in Constructing the Universe with Clusters of Galaxies
Feretti, L., Fusco-Femiano, R., Giovannini, G., & Govoni, F. 2001, A&A, 373, 106
Ferrari, C., Govoni, F., Schindler, S., Bykov, A. M., & Rephaeli, Y. 2008, Space Sci. Rev., 134, 93
Finoguenov, A., Henriksen, M. J., Briel, U. G., de Plaa, J., & Kaastra, J. S. 2004, ApJ, 611, 811
Fusco-Femiano, R. 2004, Ap&SS, 294, 37
Giovannini, G., Bonafede, A., Feretti, L., et al. 2009, A&A, 507, 1257
Govoni, F., & Feretti, L. 2004, Int. J. Mod. Phys. D, 13, 1549
Govoni, F., Enßlin, T. A., Feretti, L., & Giovannini, G. 2001, A&A, 369, 441
Govoni, F., Murgia, M., Feretti, L., et al. 2005, A&A, 430, L5
Govoni, F., Murgia, M., Feretti, L., et al. 2006, A&A, 460, 425
Govoni, F., Dolag, K., Murgia, M., et al. 2010, A&A, 522, A105
Guidetti, D., Murgia, M., Govoni, F., et al. 2008, A&A, 483, 699
Hanisch, R. J., & Erickson, W. C. 1980, AJ, 85, 183
Harris, D. E., Kapahi, V. K., & Ekers, R. D. 1980, A&AS, 39, 215
Herbig, T., & Birkinshaw, M. 1994, in BAAS, 26, 1403
Hudson, D. S., Mittal, R., Reiprich, T. H., et al. 2010, A&A, 513, A37
Jeltema, T. E., & Profumo, S. 2010, ArXiv e-prints
Johnston-Hollitt, M., Hollitt, C. P., & Ekers, R. D. 2004, in The Magnetized Interstellar Medium, ed. B. Uyaniker, W. Reich, & R. Wielebinski, 13
Kassim, N. E., Clarke, T. E., Enßlin, T. A., Cohen, A. S., & Neumann, D. M. 2001, ApJ, 559, 785
Keshet, U., & Loeb, A. 2010, ArXiv e-prints
Krempeć-Krygier, J., Krygier, B., & Krywult, J. 2002, Baltic Astron., 11, 269
Kunz, M. W., Schekochihin, A. A., Cowley, S. C., Binney, J. J., & Sanders, J. S. 2010, ArXiv e-prints
Laing, R. A., & Bridle, A. H. 1987, MNRAS, 228, 557
Laing, R. A., Bridle, A. H., Parma, P., & Murgia, M. 2008, MNRAS, 391, 521
Liang, H., Hunstead, R. W., Birkinshaw, M., & Andreani, P. 2000, ApJ, 544, 686
Markevitch, M., Mazzotta, P., Vikhlinin, A., et al. 2003, ApJ, 586, L19
Miller, N. A., & Owen, F. N. 2003, AJ, 125, 2427
Motl, P. M., Burns, J. O., Loken, C., Norman, M. L., & Bryan, G. 2004, ApJ, 606, 635
Murgia, M., Govoni, F., Feretti, L., et al. 2004, A&A, 424, 429
Murgia, M., Eckert, D., Govoni, F., et al. 2010a, A&A, 514, A76
Murgia, M., Govoni, F., Feretti, L., & Giovannini, G. 2010b, A&A, 509, A86
Narayan, R., & Medvedev, M. V. 2001, ApJ, 562, L129
Neumann, D. M., Lumb, D. H., Pratt, G. W., & Briel, U. G. 2003, A&A, 400, 811
Parrish, I. J., Quataert, E., & Sharma, P. 2009, ApJ, 703, 96
Parrish, I. J., Quataert, E., & Sharma, P. 2010, ApJ, 712, L194
Petrosian, V. 2001, ApJ, 557, 560
Pizzo, R. F., de Bruyn, A. G., Bernardi, G., & Brentjens, M. A. 2010, ArXiv e-prints
Reiprich, T. H., & Böhringer, H. 2002, ApJ, 567, 716
Reiprich, T. H., Sarazin, C. L., Kempner, J. C., & Tittley, E. 2004, ApJ, 608, 179
Rines, K., & Diaferio, A. 2006, AJ, 132, 1275
Rossetti, M., & Molendi, S. 2010, A&A, 510, A83
Rossetti, M., Ghizzardi, S., Molendi, S., & Finoguenov, A. 2007, A&A, 463, 839
Ruszkowski, M., & Oh, S. P. 2010, ApJ, 713, 1332
Ruszkowski, M., Lee, D., Bruggen, M., Parrish, I., & Oh, S. P. 2010, ApJ, submitted [arXiv:1010.2277]
Rykoff, E. S., Evrard, A. E., McKay, T. A., et al. 2008, MNRAS, 387, L28
Schuecker, P., Finoguenov, A., Miniati, F., Böhringer, H., & Briel, U. G. 2004, A&A, 426, 387
Sun, M., Murray, S. S., Markevitch, M., & Vikhlinin, A. 2002, ApJ, 565, 867
Takahashi, S., & Yamashita, K. 2003, PASJ, 55, 1105
Vacca, V., Murgia, M., Govoni, F., et al. 2010, A&A, 514, A71
van Weeren, R. J., Röttgering, H. J. A., Brüggen, M., & Hoeft, M. 2010, Science, 330, 347
Vazza, F., Brunetti, G., Kritsuk, A., et al. 2009, A&A, 504, 33
Venturi, T., Bardelli, S., Morganti, R., & Hunstead, R. W. 2000, MNRAS, 314, 594
Venturi, T., Giacintucci, S., Dallacasa, D., et al. 2008, A&A, 484, 327
Vogt, C., & Enßlin, T. A. 2005, A&A, 434, 67
Whitaker, K. E., Kraft, R. P., Posson-Brown, J., Jones, C., & Donnelly, R. H. 2003, in BAAS, 35, 1282
Wik, D. R., Sarazin, C. L., Finoguenov, A., et al. 2009, ApJ, 696, 1700